Supercond. Sci. Technol.

arXiv:0708.3379v1 [cond-mat.supr-con] 24 Aug 2007

Magnetic-field dependence of the critical currents in a periodic coplanar array of narrow superconducting strips

John R Clem,[1]§ Ali A Babaei Brojeny[2] and Yasunori Mawatari[3]

[1] Ames Laboratory and Department of Physics and Astronomy,
Iowa State University, Ames, Iowa, 50011–3160, USA
[2] Department of Physics, Isfahan University of Technology, Isfahan 84154, Iran
[3] National Institute of Advanced Industrial Science and Technology (AIST)
Tsukuba, Ibaraki 305–8568, Japan

E-mail: clem@ameslab.gov

Abstract. We calculate the magnetic-field dependence of the critical current due to both geometrical edge barriers and bulk pinning in a periodic coplanar array of narrow superconducting strips. We find that in zero or low applied magnetic fields the critical current can be considerably enhanced by the edge barriers, but in modest applied magnetic fields the critical current reduces to that due to bulk pinning alone.

PACS numbers: 74.25.Sv,74.25.Op,74.25.Qt

Submitted to: *Institute of Physics Publishing*
Supercond. Sci. Technol.

§ To whom correspondence should be addressed.

1. Introduction

The critical current at which a voltage appears along the length of a superconductor is one of the most important factors considered in applications of superconductivity [1]. The critical current is known to depend upon both local pinning centers in the material and the shape of the conductor's cross section. Even in the absence of bulk pinning, isolated type-II superconducting thin-film strips subjected to perpendicular magnetic fields show magnetic hysteresis due to geometrical edge barriers [2, 3, 4, 5, 6, 7]. Such strips have finite critical currents arising from the edge barriers [8]. It also has been shown that the critical currents become larger when slits are fabricated near the edges of the strips [9]; the edge-barrier effects are enhanced because the slits increase the number of edges that can prevent flux penetration into the inner strips. Although at subcritical applied fields and currents the magnetic response of two parallel strips in the Meissner state is reversible [10], when the strips are connected at their ends and an applied magnetic field exceeds a certain value, magnetic flux penetrates irreversibly and the magnetic response becomes hysteretic as a consequence of the edge barriers [11, 12, 13]. A detailed analysis of the effects of edge barriers upon the magnetization hysteresis in samples consisting of one, two, and three parallel strips connected at their ends has been presented in [14].

To calculate the combined effects of geometrical barriers and bulk pinning is more difficult, but this has been accomplished for single strips in [4, 5, 7, 15, 16, 17, 18, 19], and a theoretical analysis of the magnetic-field dependence of the critical current of an isolated superconducting strip due to both an edge barrier and uniform bulk pinning has been presented in [20]. Here we extend the above calculations to account for both geometrical edge barriers and bulk pinning in an infinite number of strips using the X-array method [21], by which the magnetic-field and current-density distributions for an array of parallel superconducting strips arranged periodically along the x axis in the plane $y = 0$ can be obtained analytically from the solutions for an isolated superconducting strip [20]. In particular, we consider the case for which each strip in the array carries an equal amount of current in the presence of a perpendicular applied magnetic field. We then calculate the critical current I_c of each strip accounting for both a geometrical edge barrier, which impedes the entry of vortices into the strip, and uniform bulk pinning, which impedes the motion of vortices across the strip.

Our calculation is relevant to a number of recent studies of the ac properties of striated coated-conductor tapes, i.e., tapes that have been subdivided into parallel thin strips (filaments) separated by narrow gaps. Ideally, to minimize ac losses in power engineering applications using multifilamentary conductors, the individual filaments should not only have small cross sections but also be twisted and transposed, such that the filaments are inductively equivalent, are decoupled from each other, and thus carry equal current [22]. In practice, it is not possible to satisfy all these conditions, and compromises are generally accepted for practical reasons. Carr and Oberly [23] have suggested that that the ac losses in tapes several millimeters wide

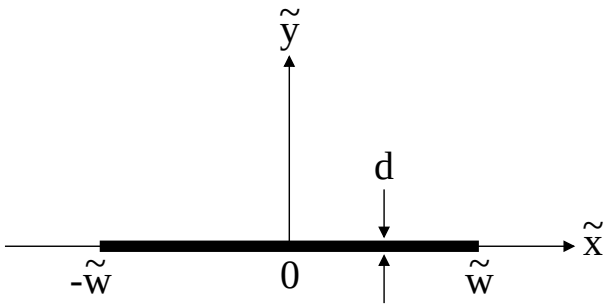


Figure 1. Long thin superconducting strip of thickness d and width $2\tilde{w}$.

could be reduced by first subdividing the tapes by striations and then twisting the tapes. Analytical and experimental results pursuing this idea have been reported in [24, 25, 26, 27, 28, 29, 30, 31, 32, 33, 34, 35, 36, 37]. Ashworth and Grilli [38] have recently proposed a variation of this approach, in which the tape is also subdivided into narrow parallel filaments, but instead of twisting the tape, the filaments are interrupted periodically by transverse cross-cuts bridged with normal metal. Magnetic flux can enter at the cross-cuts, thereby decoupling the filaments and allowing equal currents to flow in each filament. The additional ohmic losses in the normal bridges are more than compensated by a huge reduction in the far more important ac coupling losses.

In the present paper we examine the dc properties of an infinite array of parallel superconducting strips, which can be regarded as an approximation to a striated coated-conductor tape of finite width. Our paper focuses on the possibility that a geometrical edge barrier can increase the critical current of each strip above that due to bulk pinning alone, but it also should be possible to use our results in calculating the hysteretic ac losses of an array of parallel strips as in [21, 39, 40, 41].

Our paper is organized as follows. In Sec. 2 we review our complex-field approach and the X-array method. In Sec. 3 we apply the complex-field approach and the X-array method to obtain the complex field and the critical currents in a periodic array of parallel superconducting strips subject only to bulk pinning. In Sec. 4 we calculate the magnetic-field dependence of the critical current of one of the strips when the infinite array is subject only to geometrical edge barriers. In Sec. 5 we calculate the critical current of one of the strips when both geometrical edge barriers and bulk pinning are present. We discuss the results and present our conclusions in Sec. 6.

2. Complex fields and X arrays

We begin by reviewing the properties of a long superconducting strip of thickness d centered on the $\tilde{z}$ axis in the region $|\tilde{x}| < \tilde{w}$ and $|\tilde{y}| < d/2$, where $d \ll \tilde{w}$ [see figure 1]. (We attach tildes to all quantities related to the single strip.) Since we are not concerned with details of how the current density varies across the film thickness, we consider only the sheet-current density $\tilde{\boldsymbol{K}}(\tilde{x}) = \int_{-d/2}^{d/2} \tilde{\boldsymbol{j}} d\tilde{y} = \hat{z}\tilde{K}_z(\tilde{x})$. If the film thickness d is less

than the London penetration depth λ, we assume that the two-dimensional screening length (or Pearl length) [42] $\Lambda = 2\lambda^2/d$ is much smaller than $\tilde{w}$. We consider the general case when the strip carries a current in the $\tilde{z}$ direction and is subjected to a perpendicular applied field $\tilde{H}_a$ in the $\hat{y}$ direction. Outside the strip, the net magnetic field $\tilde{\boldsymbol{H}}(\tilde{x},\tilde{y}) = \hat{x}\tilde{H}_x(\tilde{x},\tilde{y}) + \hat{y}\tilde{H}_y(\tilde{x},\tilde{y})$ obeys $\tilde{\nabla}\times\tilde{\boldsymbol{H}} = 0$ and $\tilde{\nabla}\cdot\tilde{\boldsymbol{H}} = 0$.

For a two-dimensional problem such as this, it is convenient to introduce a complex magnetic field $\tilde{H}(\tilde{\zeta}) = \tilde{H}_y(\tilde{x},\tilde{y}) + i\tilde{H}_x(\tilde{x},\tilde{y})$, which is an analytic function of the complex variable $\tilde{\zeta} = \tilde{x} + i\tilde{y}$ outside the strip. The real and imaginary parts of $\tilde{H}(\tilde{\zeta})$ obey the Cauchy relations, $\partial\tilde{H}_y/\partial\tilde{x} = \partial\tilde{H}_x/\partial\tilde{y}$ and $\partial\tilde{H}_y/\partial\tilde{y} = -\partial\tilde{H}_x/\partial\tilde{x}$, which guarantee that $\tilde{\boldsymbol{H}}$ obeys $\tilde{\nabla}\times\tilde{\boldsymbol{H}} = 0$ and $\tilde{\nabla}\cdot\tilde{\boldsymbol{H}} = 0$, respectively. The Biot-Savart law can be expressed as

$$\tilde{H}(\tilde{\zeta}) = \tilde{H}_a + \frac{1}{2\pi}\int_{-\tilde{w}}^{\tilde{w}} \frac{\tilde{K}_z(\tilde{u})d\tilde{u}}{\tilde{\zeta}-\tilde{u}}. \tag{1}$$

Using the property that $1/(x \pm i\epsilon) = (P/x) \mp i\delta(x)$, where ϵ is a positive infinitessimal and P denotes the principal value, we obtain

$$\tilde{H}_y(\tilde{x},0) = \tilde{H}_a + \frac{P}{2\pi}\int_{-\tilde{w}}^{\tilde{w}} \frac{\tilde{K}_z(\tilde{u})d\tilde{u}}{\tilde{x}-\tilde{u}} \tag{2}$$

and

$$\begin{aligned}\tilde{H}_x(\tilde{x},\pm\epsilon) &= \mp\tilde{K}_z(\tilde{x})/2, \quad |\tilde{x}| < \tilde{w},\\ &= 0, \quad \text{otherwise.}\end{aligned} \tag{3}$$

The net current carried in the $\tilde{z}$ direction is

$$\tilde{I}_z = \int_{-\tilde{w}}^{\tilde{w}} \tilde{K}_z(\tilde{x})d\tilde{x}. \tag{4}$$

Note from (1) that an expansion of $\tilde{H}(\tilde{\zeta})$ in powers of $1/\tilde{\zeta}$ yields [14] $\tilde{H}(\tilde{\zeta}) = \tilde{H}_a + \tilde{I}_z/2\pi\tilde{\zeta} + \mathrm{O}(1/\tilde{\zeta}^2)$.

Solutions for the magnetic-field and current-density distributions for a long thin strip are known for many different physical situations. It has been shown by Mawatari in [21] how known solutions $\tilde{H}(\tilde{\zeta})$ and $\tilde{K}_z(\tilde{x})$ for a single isolated strip can be used to generate the corresponding solutions $H(\zeta)$ and $K_z(x)$ for an X array, i.e., an infinite periodic array of identical coplanar strips of width $2w$ and periodicity L in the plane $y = 0$, as sketched in figure 2. The complex field $H(\zeta) = H_y(x,y) + iH_x(x,y)$, which is an analytic function of the complex variable $\zeta = x + iy$ outside the strips, describes the components of the net magnetic field $\boldsymbol{H}(x,y) = \hat{x}H_x(x,y) + \hat{y}H_y(x,y)$ produced by a sheet-current density $\boldsymbol{K}(x) = \hat{z}K_z(x)$ and a magnetic field H_a applied in the y direction. The periodicity requires that the magnetic field and sheet-current density obey $\boldsymbol{H}(x+L,y) = \boldsymbol{H}(x,y)$ and $\boldsymbol{K}(x+L) = \boldsymbol{K}(x)$.

Corresponding solutions for the periodic complex field $H(\zeta)$ can be obtained from $\tilde{H}(\tilde{\zeta})$ using the conformal mapping [21]

$$\tilde{\zeta} = (L/\pi)\tan(\pi\zeta/L), \tag{5}$$

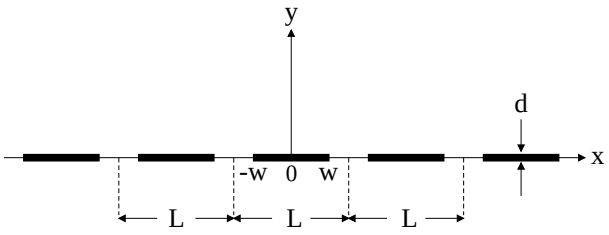


Figure 2. X array of long thin superconducting strips of thickness d, width $2w$, periodicity L, and separation $\Delta = L - 2w$.

or its inverse

$$\zeta = (L/\pi)\arctan(\pi\tilde{\zeta}/L). \tag{6}$$

These equations also describe the relations between $\tilde{x}$ and x, $\tilde{w}$ and w, or $\tilde{u}$ and u, which will appear in later expressions. Then $H(\zeta) = \tilde{H}(\tilde{\zeta})$, $K_z(x) = \tilde{K}_z(\tilde{x})$, and the Biot-Savart law yields [21]

$$H(\zeta) = H_a + \frac{1}{2L}\int_{-w}^{w} K_z(u)\cot\Big[\frac{\pi(\zeta-u)}{L}\Big]du, \tag{7}$$

where the magnetic field applied in the y direction in the ζ plane is [21]

$$H_a = \tilde{H}_a - \frac{1}{2\pi}\int_{-\tilde{w}}^{\tilde{w}} \frac{\tilde{K}_z(\tilde{u})\tilde{u}d\tilde{u}}{(L/\pi)^2 + \tilde{u}^2} \tag{8}$$

and the current carried in the z direction by one of the strips shown in figure 2 is

$$I_z = \int_{-w}^{w} K_z(x)dx. \tag{9}$$

Note by comparing (4) and (9) that I_z is in general not the same as $\tilde{I}_z$. The relations (8) and (9) can be obtained from (7) by applying the requirement that

$$H(\pm i\infty) = \tilde{H}(\pm iL/\pi) = H_a \mp iI_z/2L. \tag{10}$$

Along the x axis, we have the properties $H(x \pm i\epsilon) = \tilde{H}(\tilde{x} \pm i\epsilon)$, $H_x(x \pm i\epsilon) = \mp K_z(x)/2$, and

$$H_y(\pm L/2, 0) = \tilde{H}_a = H_a + \frac{1}{2L}\int_{-w}^{w} K_z(u)\tan(\frac{\pi u}{L})du. \tag{11}$$

In the following sections, we shall obtain $H(\zeta)$ using $H(\zeta) = \tilde{H}(\tilde{\zeta})$, $K_z(x) = \tilde{K}_z(\tilde{x})$, (5) and (10), and various trigonometric identities.

3. Critical current due only to bulk pinning

When the critical current of a single superconducting strip is due solely to bulk pinning, characterized by the bulk-pinning critical current density J_p (here assumed to be field-independent, an assumption to be justified in Sec. 6), the corresponding critical sheet-

current density is $K_p = J_p d$, and $\tilde{K}_z = K_p$ for $|\tilde{x}| < \tilde{w}$, such that the critical current is $\tilde{I}_p = 2K_p\tilde{w}$ and the complex field is

$$\tilde{H}(\tilde{\zeta}) = \tilde{H}_a + \frac{K_p}{2\pi}\ln\Big(\frac{\tilde{\zeta}+\tilde{w}}{\tilde{\zeta}-\tilde{w}}\Big). \tag{12}$$

The corresponding complex field surrounding the X array shown in figure 2 is

$$H(\zeta) = H_a + \frac{K_p}{2\pi}\ln\Big[\frac{\sin\left[\pi(\zeta+w)/L\right]}{\sin\left[\pi(\zeta-w)/L\right]}\Big], \tag{13}$$

where $H_a = \tilde{H}_a = H_y(\pm L/2, 0)$. Since $K_z = \tilde{K}_z = K_p$, we immediately find for one of the strips in the X array that its critical current is $I_p = 2K_p w$, its average critical sheet-current density is K_p, and its average critical current density is J_p. Note that when $w < L/2$, the self-field contribution to $H_y(x, 0)$ is positive and diverges logarithmically when $x \to w$; it is negative and has a similar divergence when $x \to -w$. In the limit that $w \to L/2$, however, we recover the complex potential generated by an infinite film carrying a sheet current $K_z = K_p$ in a perpendicular applied field H_a,

$$H(\zeta) = H_a \mp iK_p/2, \tag{14}$$

where the upper (lower) sign holds when $y > 0$ ($y < 0$).

4. Critical current due only to edge barriers

Consider a single bulk-pinning-free superconducting strip in which the critical current is determined by a geometrical edge barrier (or surface barrier at the edge). As discussed in [5], the current and field distributions at the critical current have two possible forms, depending upon the strength of the applied field $\tilde{H}_a$. For small values of $\tilde{H}_a$, the distributions are simply the Meissner response to the applied field and current, but for larger values of $\tilde{H}_a$, there is a domelike magnetic field distribution inside the strip.

The complex magnetic field describing the Meissner response to a magnetic field $\tilde{H}_a$ applied in the $\tilde{y}$ direction and to a net current $\tilde{I}$ applied in the z direction is [5]

$$\tilde{H}(\tilde{\zeta}) = \frac{\tilde{H}_a\tilde{\zeta} + \tilde{I}/2\pi}{(\tilde{\zeta}^2 - \tilde{w}^2)^{1/2}}, \tag{15}$$

and the sheet-current density in the strip ($|\tilde{x}| < \tilde{w}$) is

$$\tilde{K}_z(\tilde{x}) = \frac{2\tilde{H}_a\tilde{x} + \tilde{I}/\pi}{(\tilde{w}^2 - \tilde{x}^2)^{1/2}}. \tag{16}$$

If the strip contains a domelike magnetic-flux distribution in the region $\tilde{a} < \tilde{x} < \tilde{b}$, where the sheet-current density is zero, the complex magnetic field is [5]

$$\tilde{H}(\tilde{\zeta}) = \tilde{H}_a\Big[\frac{(\tilde{\zeta}-\tilde{a})(\tilde{\zeta}-\tilde{b})}{\tilde{\zeta}^2 - \tilde{w}^2}\Big]^{1/2}, \tag{17}$$

the sheet-current density in the strip ($|\tilde{x}| < \tilde{w}$) is

$$\begin{aligned}\tilde{K}_z(\tilde{x}) &= 2\tilde{H}_a\sqrt{\frac{(\tilde{x}-\tilde{a})(\tilde{x}-\tilde{b})}{\tilde{w}^2-\tilde{x}^2}}, \quad \tilde{b} < \tilde{x} < \tilde{w}, \\ &= -2\tilde{H}_a\sqrt{\frac{(\tilde{a}-\tilde{x})(\tilde{b}-\tilde{x})}{\tilde{w}^2-\tilde{x}^2}}, \quad -\tilde{w} < \tilde{x} < \tilde{a}, \\ &= 0, \quad \text{otherwise,}\end{aligned} \tag{18}$$

and the net current in the $\tilde{z}$ direction is [5]

$$\tilde{I} = -\pi(\tilde{a}+\tilde{b})\tilde{H}_a. \tag{19}$$

The corresponding quantities for the X array are, for the Meissner response to an applied field H_a in the y direction and an applied current I in the z direction, the complex field

$$H(\zeta) = \frac{H_a\sin(\frac{\pi\zeta}{L}) + (I/2L)\cos(\frac{\pi\zeta}{L})}{[\sin(\frac{\pi(\zeta+w)}{L})\sin(\frac{\pi(\zeta-w)}{L})]^{1/2}} \tag{20}$$

and the sheet-current density in the strip ($|x| < w$)

$$K_z(x) = \frac{2H_a\sin(\frac{\pi x}{L}) + (I/L)\cos(\frac{\pi x}{L})}{\sqrt{\sin(\frac{\pi(w+x)}{L})\sin(\frac{\pi(w-x)}{L})}}, \tag{21}$$

where $\tilde{H}_a = H_a/\cos(\pi w/L) = H_y(\pm L/2, 0)$ and $\tilde{I} = I/\cos(\pi w/L)$.

If all the strips in the X array contain domelike magnetic-flux distributions identical to the one in the region $a < x < b$, the complex field is

$$H(\zeta) = \frac{H_a}{\cos(\frac{\pi(a+b)}{2L})}\left[\frac{\sin(\frac{\pi(\zeta-a)}{L})\sin(\frac{\pi(\zeta-b)}{L})}{\sin(\frac{\pi(\zeta+w)}{L})\sin(\frac{\pi(\zeta-w)}{L})}\right]^{1/2}, \tag{22}$$

the sheet-current density in the central strip ($|x| < w$) is

$$\begin{aligned}K_z(x) &= \frac{2H_a}{\cos(\frac{\pi(a+b)}{2L})}\sqrt{\frac{\sin(\frac{\pi(x-a)}{L})\sin(\frac{\pi(x-b)}{L})}{\sin(\frac{\pi(w+x)}{L})\sin(\frac{\pi(w-x)}{L})}}, \\ &\qquad\qquad b < x < w, \\ &= -\frac{2H_a}{\cos(\frac{\pi(a+b)}{2L})}\sqrt{\frac{\sin(\frac{\pi(a-x)}{L})\sin(\frac{\pi(b-x)}{L})}{\sin(\frac{\pi(w+x)}{L})\sin(\frac{\pi(w-x)}{L})}}, \\ &\qquad\qquad -w < x < a, \\ &= 0, \quad \text{otherwise,}\end{aligned} \tag{23}$$

where

$$\tilde{H}_a = \frac{H_a\sqrt{\cos(\frac{\pi a}{L})\cos(\frac{\pi b}{L})}}{\cos(\frac{\pi(a+b)}{2L})\cos(\frac{\pi w}{L})} = H_y(\pm L/2, 0), \tag{24}$$

and the net current in the z direction in the strip $|x| < w$ is

$$I = -2LH_a\tan[\pi(a+b)/2L]. \tag{25}$$

The divergences in the above expressions for H and K_z at $x = \pm w$ are artifacts of ignoring the finite thickness d of the film. It is well known that these divergences are cut off at a length scale Λ_c, the larger of $\Lambda = 2\lambda^2/d$ and $d/2$ [i.e., $\Lambda_c = \max(\Lambda, d/2)$]. To determine the critical current of one of the strips of the X array, we use the approximations applied in [20] and [43]. Accordingly, we estimate the the sheet-current density at an edge by evaluating the diverging inverse square root in the expression for K_z at a distance Λ_c from that edge; for example, for the edge at $x = w$, in (21) and (23) we replace x by w in the numerators and by $x_c = w - \Lambda_c$ in the denominators and use the fact that the cut-off length scale obeys $\Lambda_c \ll w$. To account for the edge barrier, we assume that vortices nucleate and enter the superconductor when the magnitude of K_z at either edge of the strip reaches the critical value $K_s = j_s d$ at which the barrier is overcome. For an ideal edge, j_s is equal to the Ginzburg-Landau depairing current density j_{GL} [44, 45], but for an extremely defected edge, j_s may become very small. Applying this procedure to (21) for $H_a = 0$, we obtain the following approximation to the zero-field surface-barrier critical current for any one of the strips in the X array,

$$I_s(0) \equiv I_{s0} = K_s(2\pi\Lambda_c L \tan\theta)^{1/2}, \tag{26}$$

where $\theta = \pi w/L$. Alternatively, by estimating the local magnetic field at the edge of the strip [5, 43], one obtains (26) but with $K_s \approx 2H_s$, where H_s is the critical field at which the barrier is overcome. We expect that H_s is at least as large as the lower critical field H_{c1}, but under favorable circumstances it may approach the bulk thermodynamic critical field H_c.

As a function of the applied field H_a, the surface-barrier critical current is found from (21) to obey

$$I_s(H_a)/I_s(0) = 1 - h \tag{27}$$

for small h, where

$$h = H_a/(I_{s0}/2L\tan\theta). \tag{28}$$

When $L \to \infty$, (26) and (27) reduce to corresponding results found in [5] and [20] in low fields for isolated bulk-pinning-free strips.

In the linear region of $I_s(H_a)$ given in (27), the flux flow producing the voltage at a current just above I_s can be described as the nucleation of vortices at $x = w$ as they overcome the geometrical edge barrier, followed by rapid motion across the strip and annihilation at $x = -w$. This can occur only when $K_z(x) > 0$ for all $|x| < w$. For increasing H_a, however, as can be seen from (21), $K_z(-w)$ becomes zero at the critical current $I_s(H_a)$ when $H_a = I_s(H_a)/2L\tan\theta$. Combining this condition with (27), we find that this occurs when $H_a = H_{d0}$, where

$$H_{d0} = I_{s0}/4L\tan\theta, \tag{29}$$

and the subscripts $(d0)$ denote the onset of a dome for zero bulk pinning. Note that we also may write $h = H_a/2H_{d0}$. The linear portion of $I_s(H_a)$ vs H_a given in (27) ends when $H_a = H_{d0}$ or $h = h_{d0} \equiv 1/2$.

For applied fields $H_a > H_{d0}$ (or $h > h_{d0} = 1/2$), each strip contains a domelike magnetic field distribution at the critical current, and $I_s(H_a)$ is no longer a linear function of H_a. The flux flow producing the voltage at a current just above I_s can be described as the nucleation of vortices at $x = w$, as they overcome the geometrical edge barrier, followed by rapid motion from $x = w$ to $x = b$, the right boundary of the magnetic field dome. The vortices inside the dome move collectively very slowly, and vortices at $x = a \approx -w$ get pushed out of the dome and annihilate at $x = -w$. We therefore calculate the critical current by setting $a = -w$ in (23), evaluating K_z at $x = w$ using the above approximation method, and setting it equal to K_s. Using (26) and (28) we then find that the value of b at the critical current is b_c, where

$$\tan[\pi(w - b_c)/2L] = \tan(\pi w/L)/4h^2. \tag{30}$$

(Note that $b_c = -w$ when $h = 1/2$.) Substituting this into (25), we obtain $I_s(H_a)$ for $H_a \geq H_{d0}$ (or $h \geq h_{d0} = 1/2$). The critical current of one of the strips of the X array is thus given by

$$\begin{aligned} \frac{I_s(H_a)}{I_{s0}} &= 1 - h, \quad 0 \leq h \leq h_{d0} = \frac{1}{2}, \\ &= \frac{1}{4h}, \quad h_{d0} = \frac{1}{2} \leq h < h_{max}, \end{aligned} \tag{31}$$

when there is no bulk pinning and the critical current is determined only by a geometrical edge barrier (surface barrier). We expect our theory to be accurate only at sufficiently low applied fields that $h < h_{max}$ or $H_a < H_{max}$, where h_{max} is the reduced field at which $b_c = w - \Lambda_c$. From (30) we obtain $h_{max} = [(L/2\pi\Lambda_c)\tan\theta]^{1/2} \geq (w/2\Lambda_c)^{1/2} \gg 1$ and $H_{max} \approx K_s/2$.

5. Critical current due to both edge barriers and bulk pinning

In this section we calculate the complex fields and critical current I_c of one of the strips in the X array when the critical current is due not only to a geometrical edge barrier but also bulk pinning, characterized by a bulk-pinning field-independent critical sheet-current density K_p. An important parameter is the ratio‖

$$p = \frac{I_p}{I_{s0}} \frac{\sin\theta}{\theta}, \tag{32}$$

where $I_p = 2K_p w$ [see Sec. 3] is the critical current due to bulk pinning in the absence of an edge barrier, I_{s0} [see Sec. 4] is the critical current due to the edge barrier in the absence of bulk pinning when $H_a = 0$, and $\theta = \pi w/L$.

5.1. Region I: One vortex-free zone with no domes

We first consider the case of relatively weak bulk pinning when $p < 2/\pi$. In low fields ($0 < H_a < H_d$ or $0 < h < h_d$, region I of figure 3), vortices nucleate at the right edge

‖ In the limit $L \to \infty$, $p = I_p/I_{s0}$ as in [20].

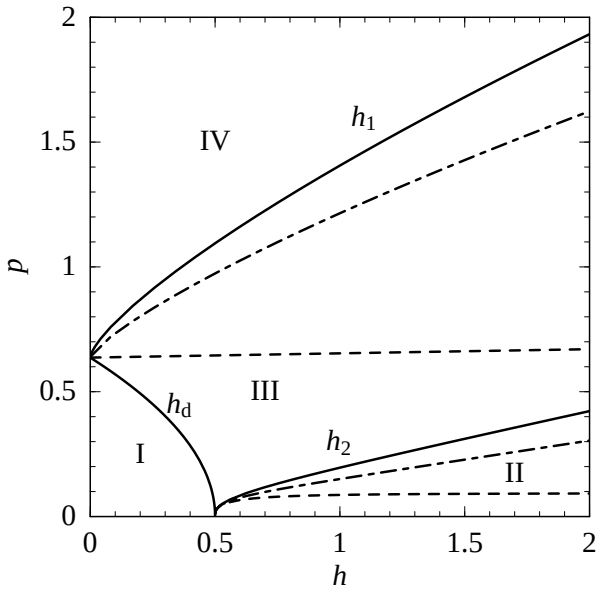


Figure 3. Diagram showing the behavior at the critical current vs reduced field h and bulk pinning parameter p. In region I, the strip is vortex-free [$H_y(x,0) = 0$]. In region II, there are two zones: a vortex dome ($-w < x < b$) and a vortex-free zone ($b < x < w$). In region III, there are three zones: a vortex dome ($a < x < b$) between two vortex-free zones ($-w < x < a$ and $b < x < w$). In region IV, there are four zones: an antivortex dome ($a < x < c$) where $H_y(x,0) < 0$, a vortex dome ($c < x < b$) where $H_y(x,0) > 0$, and two vortex-free zones ($-w < x < a$ and $b < x < w$). In each vortex-free zone $K_z(x) > K_p$, and under each vortex dome $K_z = K_c$. The curve $h_d(p)$ separates regions I and III, the curves $h_1(p,\theta)$ separate regions III and IV, and the curves $h_2(p,\theta)$ separate regions II and III. These curves are shown for $\theta = \pi w/L = 0$ (solid), $\theta = 0.5\pi/2$ (dot-dashed), and $\theta = 0.99\pi/2$ (dashed).

of the strip ($x = w$) when I_z slightly exceeds $I_s(H_a)$. When $K_z(x)$ in (21) is greater than K_p for all x in the strip ($|x| < w$), nucleating vortices are driven entirely across the strip to the opposite side at $x = -w$, where they annihilate. The critical current is then $I_c(H_a, p, \theta) = I_s(H_a)$, and the normalized critical current is

$$i_c(h, p, \theta) = I_c(H_a, p, \theta)/I_{s0} = 1 - h, \tag{33}$$

the same result as in (27). Thus if p is small, the critical current $I_c(H_a, p, \theta)$ for small H_a is still completely dominated by the edge barrier and is independent of the strength of the bulk pinning. From (21) we see that $K_z(x)$ vs x has a minimum, $K_z(x_{\min})$, at $x = x_{\min}$, where

$$\tan(\pi x_{\min}/L) = -(2LH_a/I)\tan^2(\pi w/L). \tag{34}$$

The minimum deepens [i.e., $K_z(x_{\min})$ decreases] with increasing H_a, and $K_z(x_{\min}) = K_p$ when $I = I_c(H_a, p, \theta)$ and $H_a = H_d$ or $h = h_d$, such that

$$\tan(\pi x_{\min}/L) = -[h_d/(1 - h_d)]\tan\theta, \tag{35}$$

where

$$h_d = \frac{H_d}{I_{s0}/2L\tan\theta} = \frac{1}{2}[1-(\frac{\pi p}{2})^2]. \tag{36}$$

As a result, for small $p < 2/\pi$, the linear behavior of $I_c(H_a)$ vs H_a, given by $i_c(h,p,\theta)$ vs h in (33), holds only for $0 \le h \le h_d$.

When $p < 2/\pi$ and $h > h_d$, or when $p > 2/\pi$ and h has any value, i.e., for h and p outside region I of figure 3, domelike magnetic-field distributions occur at the critical current $I_c(H_a)$. Using the X-array method [21], we can obtain the complex field $H(\zeta)$ and associated sheet-current density $K_z(x)$ in one of the strips of the X array from the corresponding solution for an isolated strip [20]. For the X array, we find $H(\zeta) = \tilde{H}(\tilde{\zeta})$, where

$$\tilde{H}(\tilde{\zeta}) = \tilde{P}(\tilde{a},\tilde{b},\tilde{\zeta})[\tilde{H}_a + \frac{K_p}{2\pi}\tilde{Q}(\tilde{a},\tilde{b},\tilde{\zeta})], \tag{37}$$

where

$$\tilde{P}(\tilde{a},\tilde{b},\tilde{\zeta}) = \Big[\frac{(\tilde{\zeta}-\tilde{a})(\tilde{\zeta}-\tilde{b})}{(\tilde{\zeta}^2-\tilde{w}^2)}\Big]^{1/2}, \tag{38}$$

$$\tilde{Q}(\tilde{a},\tilde{b},\tilde{\zeta}) = \int_{\tilde{a}}^{\tilde{b}} \frac{\sqrt{\tilde{w}^2-\tilde{u}^2}}{(\tilde{\zeta}-\tilde{u})\sqrt{(\tilde{u}-\tilde{a})(\tilde{b}-\tilde{u})}}d\tilde{u} \tag{39}$$

$$= \frac{2(\tilde{w}+\tilde{a})}{\sqrt{(\tilde{w}-\tilde{a})(\tilde{w}+\tilde{b})}}\Big[\mathbf{\Pi}\Big(\frac{\tilde{b}-\tilde{a}}{\tilde{w}+\tilde{b}},\tilde{q}\Big) - \frac{(\tilde{\zeta}-\tilde{w})}{(\tilde{\zeta}-\tilde{a})}\mathbf{\Pi}\Big(\frac{(\tilde{\zeta}+\tilde{w})(\tilde{b}-\tilde{a})}{(\tilde{\zeta}-\tilde{a})(\tilde{w}+\tilde{b})},\tilde{q}\Big)\Big] \tag{40}$$

$$= -\frac{2(\tilde{w}-\tilde{b})}{\sqrt{(\tilde{w}-\tilde{a})(\tilde{w}+\tilde{b})}}\Big[\mathbf{\Pi}\Big(\frac{\tilde{b}-\tilde{a}}{\tilde{w}-\tilde{a}},\tilde{q}\Big) - \frac{(\tilde{\zeta}+\tilde{w})}{(\tilde{\zeta}-\tilde{b})}\mathbf{\Pi}\Big(\frac{(\tilde{\zeta}-\tilde{w})(\tilde{b}-\tilde{a})}{(\tilde{\zeta}-\tilde{b})(\tilde{w}-\tilde{a})},\tilde{q}\Big)\Big], \tag{41}$$

and

$$\tilde{q}^2 = \frac{2\tilde{w}(\tilde{b}-\tilde{a})}{(\tilde{w}-\tilde{a})(\tilde{w}+\tilde{b})}. \tag{42}$$

The integral in (39) is expressed in terms of complete elliptic integrals of the third kind [46, 47, 48, 49, 50] $\mathbf{\Pi}(n,k)$, where n is called either the characteristic or the parameter, and k is called the modulus. The mappings of (5) and (6) define the relations between $\tilde{\zeta}$ and ζ, $\tilde{a}$ and a, $\tilde{b}$ and b, or $\tilde{w}$ and w, and also guarantee that $H(\zeta)$ is periodic in the x direction with period L. The applied magnetic field H_a in the y direction and the current I_z carried in the z direction by one of the strips shown in figure 2, obtained from (10), obey

$$H_a = \mathrm{Re}\{\tilde{P}(\tilde{a},\tilde{b},iL/\pi)[\tilde{H}_a + \frac{K_p}{2\pi}\tilde{Q}(\tilde{a},\tilde{b},iL/\pi)]\} \tag{43}$$

and

$$I_z = -2L\mathrm{Im}\{\tilde{P}(\tilde{a},\tilde{b},iL/\pi)[\tilde{H}_a + \frac{K_p}{2\pi}\tilde{Q}(\tilde{a},\tilde{b},iL/\pi)]\}, \tag{44}$$

where

$$\tilde{P}(\tilde{a},\tilde{b},iL/\pi) = \frac{\cos\theta}{\sqrt{\cos(\pi a/L)\cos(\pi b/L)}}e^{i\pi(a+b)/2L} \tag{45}$$

and $\theta = \pi w/L$.

The quantities of primary interest to us are $H_y(x,0) = \mathrm{Re}H(x)$ and $K_z(x) = -2\mathrm{Im}H(x+i\epsilon)$,

$$H_y(x,0) = \mathrm{Re}\tilde{H}(\tilde{x}) \tag{46}$$

$$= \tilde{P}_0(\tilde{a},\tilde{b},\tilde{x})[\tilde{H}_a + \frac{K_p}{2\pi}\mathrm{Re}\tilde{Q}(\tilde{a},\tilde{b},\tilde{x})], \tag{47}$$

$$\tilde{a} < \tilde{x} < \tilde{b} \text{ or } |\tilde{x}| > \tilde{w},$$

$$= 0, -\tilde{w} < \tilde{x} < \tilde{a} \text{ or } \tilde{b} < \tilde{x} < \tilde{w}. \tag{48}$$

$$K_z(x) = \tilde{K}_z(\tilde{x}) = -2\mathrm{Im}\tilde{H}(\tilde{x}+i\epsilon) \tag{49}$$

$$= -2\tilde{P}_0(\tilde{a},\tilde{b},\tilde{x})[\tilde{H}_a + \frac{K_p}{2\pi}\tilde{Q}(\tilde{a},\tilde{b},\tilde{x})], \tag{50}$$

$$-\tilde{w} < \tilde{x} < \tilde{a},$$

$$= K_p,\ \tilde{a} < \tilde{x} < \tilde{b}, \tag{51}$$

$$= +2\tilde{P}_0(\tilde{a},\tilde{b},\tilde{x})[\tilde{H}_a + \frac{K_p}{2\pi}\tilde{Q}(\tilde{a},\tilde{b},\tilde{x})], \tag{52}$$

$$\tilde{b} < \tilde{x} < \tilde{w},$$

where

$$\tilde{P}_0(\tilde{a},\tilde{b},\tilde{x}) = \sqrt{\frac{|\tilde{x}-\tilde{a}||\tilde{x}-\tilde{b}|}{|\tilde{x}^2-\tilde{w}^2|}}. \tag{53}$$

For the calculation of $H_y(x,0)$ for $a < x < b$ (i.e., $\tilde{a} < \tilde{x} < \tilde{b}$), taking the real part of $\tilde{Q}$ in (47) corresponds to taking the principal value of the integral of (39).

5.2. Region IV: Two vortex-free zones, one vortex dome, and one antivortex dome

For values of $p > 2/\pi$ [see (32)], and small values of h, i.e., for h and p in region IV of figure 3, the vortex distribution in each of the strips at the critical current can be described as a double dome, consisting of a vortex dome adjacent to an antivortex dome. Just above the critical current, vortices nucleate at $x = w$, where $K_z(x_c) = K_s$, move rapidly to the left through an otherwise vortex-free region ($b < x < w$), and then move slowly to the left through a vortex-filled region (the vortex dome), $c < x < b$. Antivortices nucleate at $x = -w$, where $K_z(-x_c) = K_s$, move rapidly to the right through an otherwise vortex-free region ($-w < x < a$), and then move slowly to the right through an antivortex-filled region (the antivortex dome), $a < x < c$. Vortices and antivortices annihilate at $x = c$, where the two domes meet and $H_y(c,0) = 0$.

Four equations must be solved simultaneously for a, b, $\tilde{H}_a$, and the critical current $I_c(H_a)$ for known values of h, p, and $\theta = \pi w/L$ in region IV of figure 3. One condition is that $K_z(w) = K_s$, which we evaluate by replacing $\tilde{x}$ in the denominator of (53) by $\tilde{x}_c$, where $x_c = w - \Lambda_c$ and $\tilde{x}_c = (L/\pi)\tan(\pi x_c/L) \approx \tilde{w} - \Lambda_c \sec^2\theta$, and by replacing $\tilde{x}$ by $\tilde{w}$ in $\tilde{Q}(\tilde{a}, \tilde{b}, \tilde{x})$ (40) and in the numerator of (53). This yields from (32) and (52)

$$\sqrt{(1-\tilde{a}')(1-\tilde{b}')}\tilde{h}\cos\theta + (1+\tilde{a}')\sqrt{\frac{1-\tilde{b}'}{1+\tilde{b}'}}\mathbf{\Pi}(\frac{\tilde{b}'-\tilde{a}'}{1+\tilde{b}'}, \tilde{q})p = 1, \tag{54}$$

where we use the normalized quantities $\tilde{a}' = \tilde{a}/\tilde{w}$ and $\tilde{b}' = \tilde{b}/\tilde{w}$, as well as the definition

$$\tilde{h} = \tilde{H}_a/(I_{s0}/2L\tan\theta). \tag{55}$$

A second condition is that $K_z(-w) = K_s$, which we evaluate in a similar manner with the help of (32), (41), and (50). The result is

$$-\sqrt{(1+\tilde{a}')(1+\tilde{b}')}\tilde{h}\cos\theta + (1-\tilde{b}')\sqrt{\frac{1+\tilde{a}'}{1-\tilde{a}'}}\mathbf{\Pi}(\frac{\tilde{b}'-\tilde{a}'}{1-\tilde{a}'}, \tilde{q})p = 1. \tag{56}$$

Equations (54) and (56) have nearly the same form as (9) and (10) in [20] and reduce exactly to those equations in the limit as $\theta = \pi w/L \to 0$ or $L \to \infty$. The third and fourth equations needed are obtained from (43) and (44), which we write in dimensionless form at $I_z = I_c$ as

$$h = \tilde{P}_1\tilde{h} + (p/2)(\tilde{P}_1\tilde{Q}_1 - \tilde{P}_2\tilde{Q}_2)\sec\theta, \tag{57}$$

$$i_c = -\cot\theta[\tilde{P}_2\tilde{h} + (p/2)(\tilde{P}_1\tilde{Q}_2 + \tilde{P}_2\tilde{Q}_1)\sec\theta], \tag{58}$$

where the real quantities $\tilde{P}_1, \tilde{P}_2, \tilde{Q}_1$ and $\tilde{Q}_2$ are defined via $\tilde{P}(\tilde{a}, \tilde{b}, iL/\pi) = \tilde{P}_1 + i\tilde{P}_2$ and $\tilde{Q}(\tilde{a}, \tilde{b}, iL/\pi) = \tilde{Q}_1 + i\tilde{Q}_2$, h, $\tilde{h}$, and p are defined via (28), (55), and (32), and $i_c(h, p, \theta) = I_c/I_{s0}$. For given values of the strip width $2w$, periodicity length L, dimensionless applied field h, and dimensionless bulk pinning strength p, numerical solutions of (54), (56), (57), and (58) yield the strip's dimensionless critical current $i_c(h, p, \theta)$ as well as the three other unknowns, $\tilde{a}$ (or a), $\tilde{b}$ (or b), and $\tilde{h}$. Shown in figure 4 (a) and (b) are sample plots of $H_y(x, 0)$ and $K_z(x)$ for h and p in region IV.

5.3. $h = 0$

Simplifications occur when calculating the self-field critical current when $p > 2/\pi$ and $H_a = 0$ ($h = 0$), for which $\tilde{a} = -\tilde{b}$ ($a = -b$) and $H_y(x, 0)$ is antisymmetric about the point $x = c = 0$. Equations (38) and (39) then can be evaluated as

$$\tilde{P}(-\tilde{b}, \tilde{b}, \tilde{\zeta}) = \Big(\frac{\tilde{b}^2 - \tilde{\zeta}^2}{\tilde{w}^2 - \tilde{\zeta}^2}\Big)^{1/2}, \tag{59}$$

$$\tilde{Q}(-\tilde{b}, \tilde{b}, \tilde{\zeta}) = 2\frac{\tilde{\zeta}}{\tilde{w}}\Big[\mathbf{K}\Big(\frac{\tilde{b}}{\tilde{w}}\Big) + \frac{(\tilde{w}^2 - \tilde{\zeta}^2)}{\tilde{\zeta}^2}\mathbf{\Pi}\Big(\frac{\tilde{b}^2}{\tilde{\zeta}^2}, \frac{\tilde{b}}{\tilde{w}}\Big)\Big], \tag{60}$$

where $\mathbf{K}(k)$ is the complete elliptic integral of the first kind of modulus k. In (43) and (44), $\tilde{P}(-\tilde{b}, \tilde{b}, iL/\pi)$ is pure real and $\tilde{Q}(-\tilde{b}, \tilde{b}, iL/\pi)$ is pure imaginary, such that

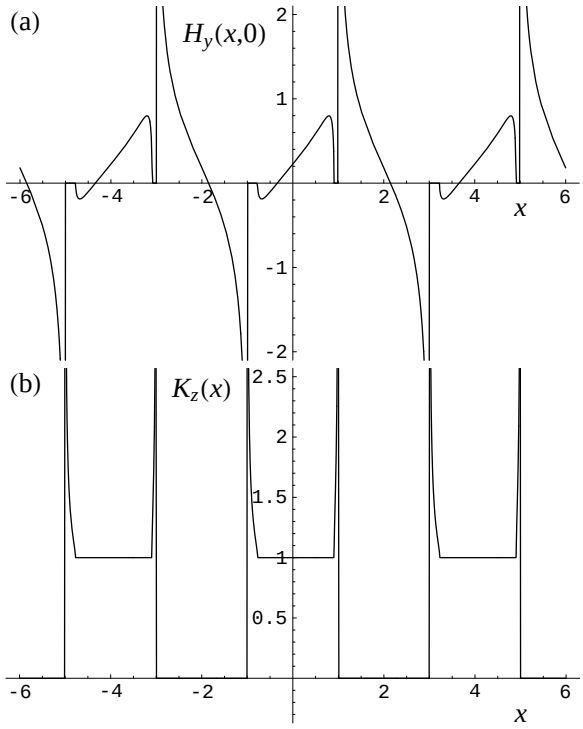


Figure 4. Plots of (a) $H_y(x,0)$ (in units of $I_{s0}/2L\tan\theta$) and (b) $K_z(x)$ (in units of K_p) vs x (in units of w) for $h = 0.2$, $p = 0.85$, and $\theta = \pi w/L = 0.5\pi/2$ (region IV), for which $i_c = I_c/I_{s0} = 1.11$ and $I_c/I_p = 1.18$, showing three strips ($-5 < x/w < -3$, $-1 < x/w < 1$, and $3 < x/w < 5$) and the gaps around them ($-7 < x/w < -5$, $-3 < x/w < -1$, $1 < x/w < 3$, and $5 < x/w < 7$).

from (57) we obtain $\tilde{h} = 0$ when $h = 0$. Equations (54) and (56), resulting from the requirement that $K_z(w) = K_z(-w) = K_s$ at the critical current, reduce to a single equation,

$$p\mathbf{K}(\tilde{b}')\sqrt{1-\tilde{b}'^2} = 1, \tag{61}$$

and the expression corresponding to (58) for the reduced critical current i_c becomes, with the help of (61),

$$i_c = \sqrt{\frac{(1-\tilde{b}'^2)}{(1+\tilde{b}'^2\tan^2\theta)}}\mathbf{\Pi}\Big(\frac{\tilde{b}'^2}{\cos^2\theta+\tilde{b}'^2\sin^2\theta},\tilde{b}'\Big)/\mathbf{K}(\tilde{b}')], \tag{62}$$

where $\theta = \pi w/L$. When $\tilde{b}' = 0$, we find that $p = 2/\pi$, and $i_c = 1$ for any value of θ. When $\theta = 0$, (62) reduces to

$$i_c = \frac{\mathbf{E}(\tilde{b}')}{\mathbf{K}(\tilde{b}')\sqrt{1-\tilde{b}'^2}}. \tag{63}$$

Plots of $H_y(x,0)$ and $K_z(x)$ vs x for $h = 0$ are similar to figure 4 (a) and (b), except that $H_y(x,0)$ is an antisymmetric function of x, centered at the origin, and $K_z(x)$ is a symmetric function of x.

5.4. h_1, the boundary between regions III and IV

For increasing values of the applied field H_a (or the reduced field h), the vortex dome expands and the antivortex dome shrinks. For reduced fields h in the range $0 \le h < h_1$, we have $H_y(x,0) < 0$ for x slightly larger than a. In other words, the coefficient of $\tilde{P}_0(\tilde{a},\tilde{b},\tilde{a}+\epsilon)$ in (47) is negative. However, when $h = h_1$, this coefficient becomes zero. For $h > h_1$, this coefficient is positive, indicating that at the critical current, only a vortex dome is present (region III in figure 3). The value of h_1 is determined chiefly by the condition that the coefficient of $\tilde{P}_0(\tilde{a},\tilde{b},\tilde{a}+\epsilon)$ in (47) is zero, which yields with the help of (41), (17.7.7) of [47], and (414.01) of [50],

$$\tilde{h} + \frac{p\sec\theta}{(\tilde{b}'-\tilde{a}')\sqrt{(1-\tilde{a}')(1+\tilde{b}')}}[(1-\tilde{a}')(1+\tilde{b}')\mathbf{E}(\tilde{q}') - (1+\tilde{a}')(1-\tilde{b}')\mathbf{K}(\tilde{q}') - (\tilde{b}'-\tilde{a}')(1-\tilde{b}')\mathbf{\Pi}(\frac{\tilde{b}'-\tilde{a}'}{1-\tilde{a}'},\tilde{q}')\Big] = 0, \tag{64}$$

where

$$\tilde{q}'^2 = \frac{2(\tilde{b}'-\tilde{a}')}{(1-\tilde{a}')(1+\tilde{b}')}. \tag{65}$$

The value of h_1 for given values of $p > 2/\pi$ and $\theta = \pi w/L$ is obtained as the value of h that satisfies (64), (54), and (56). The solutions of these equations also yield the values of $\tilde{a}'$ and $\tilde{b}'$ at the critical current when $h = h_1$.

5.5. Region III: Two vortex-free zones and one vortex dome

In region III of the diagram of p vs h shown in figure 3, at the critical current, the field and current distributions within each strip divide into three zones. For $b < x < w$, we have $H_y(x,0) = 0$ and $K_z(x) > K_c$; for $a < x < b$, we have $H_y(x,0) > 0$ and $K_z(x) = K_c$; and for $-w < x < a$, we have we have $H_y(x,0) = 0$ and $K_z(x) > K_c$. Just above the critical current I_c, the voltage along the length of the strip is produced by (a) small numbers of vortices nucleated at $x = w$ as they overcome the geometrical edge barrier, followed by their rapid motion from $x = w$ to $x = b$, (b) large numbers of vortices moving slowly through the vortex dome from $x = b$ to $x = a$, and (c) small numbers of vortices leaking out of the vortex dome and moving rapidly from $x = a$ to $x = -w$.

The four equations determining the values of a, b, $\tilde{h}$, and the reduced critical current i_c for given values of h, p and θ in region III are (54), (57), (58), and (64), since the latter equation also can be shown to give the condition that $dK_z(x)/dx = 0$ at $x = a$. Shown in figure 5 (a) and (b) are sample plots of $H_y(x,0)$ and $K_z(x)$ for h and p in region III.

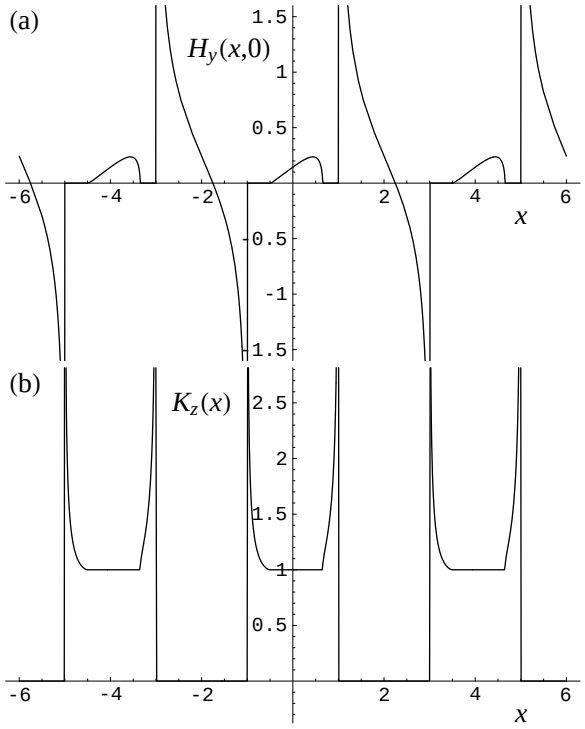


Figure 5. Plots of (a) $H_y(x,0)$ (in units of $I_{s0}/2L\tan\theta$) and (b) $K_z(x)$ (in units of K_p) vs x (in units of w) for $h = 0.2$, $p = 0.6$, and $\theta = \pi w/L = 0.5\pi/2$ (region III), for which $i_c = I_c/I_{s0} = 0.87$ and $I_c/I_p = 1.31$, showing three strips ($-5 < x/w < -3$, $-1 < x/w < 1$, and $3 < x/w < 5$) and the gaps around them ($-7 < x/w < -5$, $-3 < x/w < -1$, $1 < x/w < 3$, and $5 < x/w < 7$).

5.6. h_2, the boundary between regions III and II

For increasing values of h, the left boundary of the vortex dome moves ever closer to the left edge of the strip, i.e., $\tilde{a} \to \tilde{w}$ or $a \to -w$, and numerical difficulties arise. Although other criteria could be used, in this paper we state that for practical purposes the vortex-free zone on the left side shrinks to negligible width when $\tilde{a} = -0.9999\tilde{w}$. For given values of p and θ, this occurs at a reduced field $h = h_2$, which can be obtained by solving (54), (64), and (57) for h, $\tilde{h}$, and b after replacing $\tilde{a}$ by $-0.9999\tilde{w}$.

5.7. Region II: One vortex-free zone and one vortex dome

For values of $h > h_2$ in figure 3, all the quantities at the critical current can in principal be calculated using the same equations as for Region III. However, these quantities can be calculated with fewer numerical difficulties and with high accuracy by setting $a = -w$ in the above equations, which results in a number of simplifications. The complex field still obeys $H(\zeta) = \tilde{H}(\tilde{\zeta})$, but now, to good approximation,

$$\tilde{H}(\tilde{\zeta}) = \tilde{P}(-\tilde{w}, \tilde{b}, \tilde{\zeta})[\tilde{H}_a + \frac{K_p}{2\pi}\tilde{Q}(-\tilde{w}, \tilde{b}, \tilde{\zeta})], \tag{66}$$

where

$$\tilde{P}(-\tilde{w},\tilde{b},\tilde{\zeta}) = \Big(\frac{\tilde{\zeta}-\tilde{b}}{\tilde{\zeta}-\tilde{w}}\Big)^{1/2} \tag{67}$$

and

$$\tilde{Q}(-\tilde{w},\tilde{b},\tilde{\zeta}) = \int_{-\tilde{w}}^{\tilde{b}} \frac{\sqrt{\tilde{w}-\tilde{u}}}{(\tilde{\zeta}-\tilde{u})\sqrt{\tilde{b}-\tilde{u}}} d\tilde{u} \tag{68}$$

$$= 2\sinh^{-1}\Big(\frac{\tilde{w}+\tilde{b}}{\tilde{w}-\tilde{b}}\Big)^{1/2} - 2\Big(\frac{\tilde{\zeta}-\tilde{w}}{\tilde{\zeta}-\tilde{b}}\Big)^{1/2}\sinh^{-1}\Big[\frac{(\tilde{w}+\tilde{b})(\tilde{\zeta}-\tilde{w})}{(\tilde{w}-\tilde{b})(\tilde{\zeta}+\tilde{w})}\Big]^{1/2} \tag{69}$$

This equation is equivalent to (14b) of [20], which was misprinted without the prefactor before the second $\sinh^{-1}$ term.

$H_y(x,0) = \mathrm{Re}H(x)$ and $K_z(x) = -2\mathrm{Im}H(x+i\epsilon)$ in region II are given by

$$H_y(x,0) = \mathrm{Re}\tilde{H}(\tilde{x}) \tag{70}$$

$$= \tilde{P}_0(-\tilde{w},\tilde{b},\tilde{x})[\tilde{H}_a + \frac{K_p}{2\pi}\mathrm{Re}\tilde{Q}(-\tilde{w},\tilde{b},\tilde{x})], \tag{71}$$

$$-\tilde{w} < \tilde{x} < \tilde{b} \text{ or } |\tilde{x}| > \tilde{w},$$

$$= 0, \qquad \tilde{b} < \tilde{x} < \tilde{w}. \tag{72}$$

$$K_z(x) = \tilde{K}_z(\tilde{x}) = -2\mathrm{Im}\tilde{H}(\tilde{x}+i\epsilon) \tag{73}$$

$$= K_p, \ -\tilde{w} < \tilde{x} < \tilde{b}, \tag{74}$$

$$= +2\tilde{P}_0(-\tilde{w},\tilde{b},\tilde{x})[\tilde{H}_a + \frac{K_p}{2\pi}\tilde{Q}(-\tilde{w},\tilde{b},\tilde{x})], \ \ \tilde{b} < \tilde{x} < \tilde{w}, \tag{75}$$

where

$$\tilde{P}_0(-\tilde{w},\tilde{b},\tilde{x}) = \sqrt{\frac{|\tilde{x}-\tilde{b}|}{|\tilde{x}-\tilde{w}|}}. \tag{76}$$

Three equations must be solved simultaneously for $\tilde{b}$ (or b), $\tilde{h}$, and i_c for given values of h, p, and θ in region II of figure 3. The condition that $K_z(w) = K_s$, evaluated as in deriving (54), becomes

$$\sqrt{2(1-\tilde{b}')}\left(\tilde{h}\cos\theta + p\sinh^{-1}\sqrt{\frac{1+\tilde{b}'}{1-\tilde{b}'}}\right) = 1, \tag{77}$$

and the other two equations needed are (57) and (58), in which the real quantities $\tilde{P}_1, \tilde{P}_2, \tilde{Q}_1$ and $\tilde{Q}_2$ are defined via $\tilde{P}(-\tilde{w},\tilde{b},iL/\pi) = \tilde{P}_1 + i\tilde{P}_2$ and $\tilde{Q}(-\tilde{w},\tilde{b},iL/\pi) = \tilde{Q}_1 + i\tilde{Q}_2$. Shown in figure 6 (a) and (b) are sample plots of $H_y(x,0)$ and $K_z(x)$ for h and p in region II.

5.8. Critical current

Using the above approach, one can calculate the normalized critical current $i_c = I_c/I_{s0}$ (26) for arbitrary values of the reduced field h (28), pinning parameter p (32), and $\theta = \pi w/L$, where the strip width is $2w$ and the periodicity length is L. Shown in figure

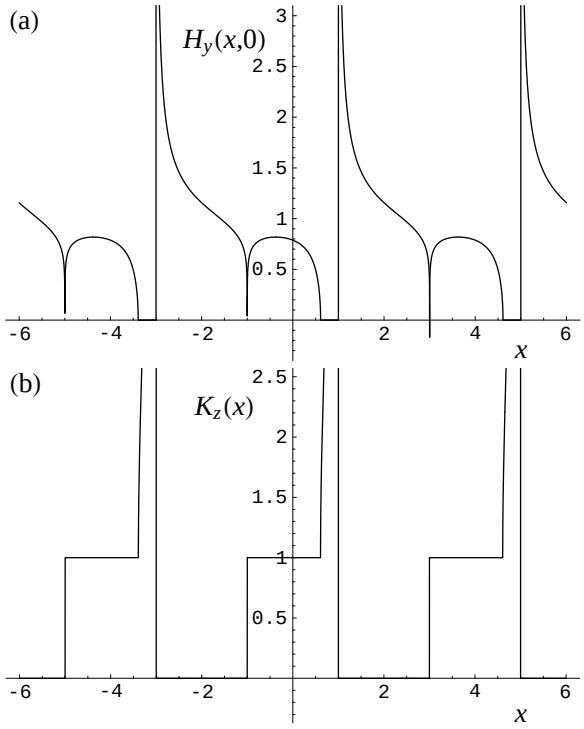


Figure 6. Plots of (a) $H_y(x,0)$ (in units of $I_{s0}/2L\tan\theta$) and (b) $K_z(x)$ (in units of K_p) vs x (in units of w) for $h = 1.0$, $p = 0.15$, and $\theta = \pi w/L = 0.5\pi/2$ (region II), for which $i_c = I_c/I_{s0} = 0.35$ and $I_c/I_p = 2.08$, showing three strips ($-5 < x/w < -3$, $-1 < x/w < 1$, and $3 < x/w < 5$) and the gaps around them ($-7 < x/w < -5$, $-3 < x/w < -1$, $1 < x/w < 3$, and $5 < x/w < 7$).

7 are sample results for $\theta = 0.5\pi/2$, when the widths of the strips and the gaps are equal. Because of the effects of the geometrical barrier, at sufficiently low applied fields and small values of p, the overall critical current I_c can be considerably enhanced above the critical current $I_p = 2wK_p$ due to bulk pinning alone. This occurs because the sheet-current density $K_z(x)$ in the vortex-free zones near the sample edges can carry a supercurrent with a density well above K_p. However, in high applied fields the cross section of the strip becomes nearly completely filled with vortices, and the sheet-current density in the vortex-filled zones cannot exceed K_p.

6. Conclusions

In this paper we have considered an infinite array (X array) of coplanar equally spaced superconducting strips and have calculated the critical current of each strip in the presence of a perpendicular applied field, taking into account not only geometrical barriers at the edges of the strips but also bulk pinning characterized by a field-independent critical sheet-current density K_p. We have carried out these calculations using the X-array method of [21], which enabled us to use solutions from [20] for an

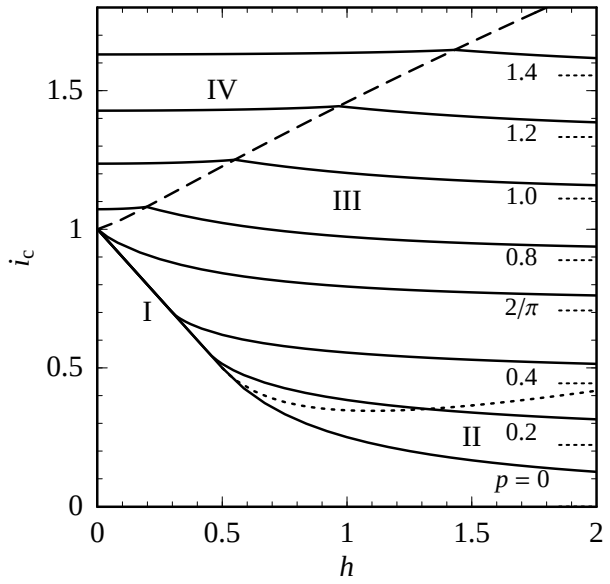


Figure 7. $i_c(h, p, \theta)$ (critical current normalized to I_{s0}) vs reduced field h for $\theta = 0.5\pi/2$ and various values of the bulk pinning parameter p. The solid curves exhibit i_c vs h, the dashed curve shows i_c at $h = h_1(p, \theta)$, and the dotted curve shows i_c at $h = h_2(p, \theta)$. For $p < 2/\pi$, i_c decreases linearly with h (33) up to h_d and then decreases more slowly in regions III and II. One curve shows i_c for the special case of $p = 2/\pi$. For $p > 2/\pi$, i_c increases by a few percent in the double-dome region IV and then decreases more gradually in regions III and II. In all cases, i_c asymptotically approaches $p\theta/\sin\theta$ for large h (short dotted lines along the right side of the figure).

isolated strip.

Geometrical barriers at the edges of the strips enhance the critical current above what it would be if it were due to bulk pinning alone. At low fields, these barriers delay the entrance of vortices and permit the strip edges to remain vortex-free and carry a sheet-current density well in excess of K_p. Any vortices and antivortices entering the strips arrange themselves into domelike distributions, and under these domes the sheet-current density remains at K_p. As the perpendicular applied field increases, more and more vortices are forced into the strip, causing the vortex domes to expand and the high-current-density vortex-free zones to shrink, such that the overall critical current approaches that due to bulk pinning alone, $I_p = 2wK_p$.

The effects predicted in this paper for parallel arrays of narrow superconducting strips would be most easily observed experimentally using magneto-optical or scanning techniques in materials with low bulk pinning, such as Bi-2212 ($Bi_2Sr_2CaCu_2O_{8+\delta}$), where geometrical-barrier effects were first observed [3, 4], or in low-pinning type-I superconductors, such as Pb, where magnetic flux domes consisting of the intermediate state have been observed [51]. However, it is important also to consider the possibility of observing these effects in materials with strong bulk pinning.

As a practical application of the above theory to coated conductors made

of superconducting YBCO ($YBa_2Cu_3O_{7-\delta}$), let us calculate the critical-current enhancement due to geometrical barriers for an isolated strip and then estimate how this enhancement is affected by striations. We first consider a long flat strip of thickness $d = 1$ μm and width $2w = 5$ mm. We assume that its self-field bulk-pinning critical current density is $J_p = 1$ MA/cm^2 (10^{10} A/m^2), such that the bulk-pinnng critical sheet-current density is $K_p = J_p d = 10^4$ A/m and the bulk-pinning critical current is $I_p = 2wK_p = 50$ A. We use (26) with $K_s = 2H_s$, $\Lambda_c = d/2$, and $L \to \infty$ to estimate the zero-field surface-barrier critical current I_{s0}. We use the experimental results of [52] as discussed in [53], from which we estimate that $H_{c1} = 180$ Oe $= 1.4 \times 10^4$ A/m and $H_c = 3.2$ kOe $= 2.6 \times 10^5$ A/m at 77 K. We use the conservative estimate that $H_s = H_{c1}$, which yields $I_{s0} = 2\pi H_{c1}\sqrt{dw} = 4.5$ A. The corresponding scaling field

$$H_{scale} = I_{s0}/2L\tan\theta, \tag{78}$$

which appears in the denominator of (28) and (55), becomes $H_{scale} = H_{c1}\sqrt{d/w} = 3.6$ Oe $= 286$ A/m. The corresponding value of the pinning parameter is $p = 11$, for which we obtain from (61) and (63) that the self-field critical current I_c at $h = H_a/H_{scale} = 0$ is very nearly equal to I_p. Moreover, I_c remains very nearly equal to to I_p as the applied field increases. Our solutions show that the vortex-free regions are very close to the edges at the critical current (i.e., b and $-a$ are nearly equal to w), such that the geometrical-barrier enhancement of I_c is negligible.

Next we suppose that the 5 mm strip is subdivided into 50 parallel strips, each of width $2w = 98$ μm, separated by gaps of width 2 μm, with period $L = 100$ μm. To approximate the behavior of the resulting striated conductor, we apply the above X-array results. Using (26) with $K_s = 2H_s$, $\Lambda_c = d/2$, $\theta = \pi w/L = 0.49\pi$, and $\tan\theta = 31.8$, we find that the zero-field surface-barrier critical current of one of the narrow strips is $I_{s0} = 2H_{c1}(\pi dL\tan\theta)^{1/2} = 2.9$ A. The corresponding bulk-pinning critical current is $I_p = 2wK_p = 0.98$ A, and the bulk-pinning parameter (32) is $p = 0.22$. Since $p < 2/\pi$, the reduced critical current is $i_c = 1$, and the self-field critical current of one of the strips is $I_c = I_{s0} = 2.9$ A, determined by the geometrical barrier alone. Since there are 50 such strips, the estimated total self-field critical current is 143 A. The corresponding engineering critical current density, taking the cross section to be 5 mm $\times$ 1 μm (ignoring the cross section of the substrate) is $J_e = 2.9 \times 10^{10}$ A/m^2 $=$ 2.9 MA/cm^2, as opposed to the 1 MA/am^2 critical current density for the unstriated strip. The reduced critical current i_c vs h for this case is similar to that shown in figure 7 for $p = 0.2$. However, the scaling field for i_c vs h from (78) is small: $H_{scale} = 5.7$ Oe $=$ 450 A/m. To summarize, the X-array results using the above assumptions predict that the self-field critical current for the striated conductor can be significantly enhanced above that due to bulk-pinning alone (by approximately a factor of three using the above numbers). However, the application of a relatively small perpendicular magnetic field (of the order of tens of Oe or hundreds of A/m using the above numbers) can be expected to produce a strong reduction of the enhancement and to return the critical current nearly to that due to bulk-pinning alone.

Throughout this paper we have assumed that the bulk-pinning critical current density J_p is field-independent. We now justify this assumption as follows. We see from figure 7 that the critical current has a significant dependence upon $h = H_a/H_{scale} = B_a/B_{scale}$ only when $h \sim 1$. In the above two paragraphs we found for state-of-the-art YBCO coated conductors for which $J_p \sim 1$ MA/cm^2 (10^{10} A/m^2) that $H_{scale} < 10$ Oe $= 796$ A/m or $B_{scale} = \mu_0 H_{scale} < 10$ G $= 1$ mT. Experimentally it has been found, for example in [54, 55], that J_p at 77 K in strong-pinning YBCO films is very nearly independent of field for $H_a < 100$ Oe ≈ 8000 A/m or $B_a < 100$ G $= 10$ mT. Therefore it is an excellent approximation to assume that J_p is field-independent over the range of applied fields for which the effects of geometrical barriers or edge pinning are relevant.

In [53], we argued that in state-of-the art unstriated YBCO coated conductors the pinning is due almost entirely to bulk pinning and that geometrical barriers (or edge pinning) have a negligible effect upon the critical current. The above calculations indicate that for striated coated conductors the additional edges produced by the striations could produce significant enhancements of the critical current in self-field, but these enhancements are strongly suppressed by relatively small applied magnetic fields. In applications where the magnetic flux density is of the order of 0.1 T or higher, where J_p has a strong field dependence, we expect that geometrical barriers will have no significant effect upon YBCO coated conductors, even if they are striated.

Acknowledgments

We thank I. L. Maksimov for stimulating discussions. This manuscript has been authored in part by Iowa State University of Science and Technology under Contract No. DE-AC02-07CH11358 with the U.S. Department of Energy.

References

[1] Campbell A M and Evetts J E 1972 *Critical Currents in Superconductors* (Taylor & Francis, London)
[2] Indenbom M V, Kronmüller H, Li T W, Kes P H and Menovsky A A 1994 *Physica C* **222** 203
[3] Schuster Th, Indenbom M V, Kuhn H, Brandt E H and Konczykowski M 1994 *Phys. Rev. Lett.* **73** 1424
[4] Zeldov E, Larkin A I, Geshkenbein V B, Konczykowski M, Majer D, Khaykovich B, Vinokur V M and Shtrikman H 1994 *Phys. Rev. Lett.* **73** 1428
[5] Benkraouda M and Clem J R 1996 *Phys. Rev. B* **53** 5716
[6] Doyle T B, Labusch R and Doyle R A 1997 *Physica C* **290** 148
[7] Maksimov I L and Elistratov A A 1998 *Appl. Phys. Lett.* **72** 1650
[8] Benkraouda M and Clem J R 1998 *Phys. Rev. B* **58** 15103
[9] Mawatari Y and Clem J R 2001 *Phys. Rev. Lett.* **86** 2870
[10] Babaei Brojeny A A, Mawatari Y, Benkraouda M and Clem J R 2002 *Supercond. Sci. Technol.* **15** 1454
[11] Zhelezina N V and Maksimova G M 2002 *Tech. Phys. Lett.* **28** 618
[12] Ainbinder R M and Maksimova G M 2003 *Supercond. Sci. Technol.* **16** 871
[13] Maksimova G M, Zhelezina N V and Maksimov I L 2004 *Physica C* **402** 53

[14] Mawatari Y and Clem J R 2003 *Phys. Rev. B* **68** 0204505
[15] Maksimov I L 1995 *Europhys. Lett.* **32** 753
[16] Maksimov I L and Elistratov A A 1995 *JETP Lett.* **61** 208
[17] Elistratov A A and Maksimov I L 2000 *Phys. Solid State* **42** 201
[18] Maksimova G M, Zhelezina N V and Maksimov I L 2001 *Europhys. Lett.* **53** 639
[19] Kupriyanov M Yu and Likharev K K 1974 *Fiz. Tverd. Tela* **16** 2829 (1975 *Sov. Phys. Solid State* **16** 1835)
[20] Elistratov A A, Vodolazov D Yu, Maksimov I L and Clem J R 2002 *Phys. Rev. B* **66** 220506(R); 2003 *Phys. Rev. B* **67** 099901(E)
[21] Mawatari Y 1996 *Phys. Rev. B* **54** 13215
[22] Wilson M N 1983 *Superconducting Magnets* (Clarendon Press, Oxford) section 7.3
[23] Carr W J Jr and Oberly C E 1999 *IEEE Trans. Appl. Supercond.* **9** 1475
[24] Oberly C E, Long L, Rhoads G L and Carr W J Jr 2001 *Cryogenics* **41** 117
[25] Cobb C B, Barnes P N, Haugan T J, Tolliver J, Lee E, Sumption M, Collings E and Oberly C E 2002 *Physica C* **382** 52
[26] Polak M, Krempasky L, Chromik S, Wehler D and Moenter B 2002 *Physica C* **372-376** 1830
[27] Amemiya N, Kasai S, Yoda K, Jiang Z, Levin G A, Barnes P N and Oberly C E 2004 *Supercond. Sci. Technol.* **17** 1464
[28] Barnes P N and Sumption M D 2004 *J. Appl. Phys.* **96** 6550
[29] Levin G A, Barnes P N, Amemiya N, Kasai S, Yoda K, Jiang Z and Polyanksii A 2005 *J. Appl. Phys.* **98** 113909
[30] Wang L B, Price M B, Young J L, Kwon C, Levin G A, Haugan T J and Barnes P N 2005 *Physica C* **419** 79
[31] Sumption M D, Barnes P N and Collings E W 2005 *IEEE Trans. Appl. Supercond.* **15** 2815
[32] Majoros M, Glowacki B A, Campbell A M, Levin G A, Barnes P N and Polak M 2005 *IEEE Trans. Appl. Supercond.* **15** 2819
[33] Tsukamoto O, Sekine N, Ciszek M and Ogawa J 2005 *IEEE Trans. Appl. Supercond.* **15** 2823
[34] Levin G A, Barnes P N, Kell J W, Amemiya N, Jiang Z, Yoda K and Kimura F 2006 *Appl. Phys. Lett.* **89** 012506
[35] Demencik E, Usak P, Takacs S, Vavra I, Polak M, Levin G A and Barnes P N 2007 *Supercond. Sci. Technol.* **20** 87
[36] Polak M, Usak E, Jansak L, Demencik E, Levin G A, Barnes P N, Wehler D and Moenter B 2006 *Preprint* cond-mat/0602422
[37] Levin G A, Barnes P N and Amemiya N 2006 *Preprint* cond-mat/0609480
[38] Ashworth S P and Grilli F 2006 *Supercond. Sci. Technol.* **19** 237
[39] Mawatari Y 1997 in *Advances in Superconductivity IX*, ed Nakajima S and Murakami M (Springer, Tokyo) p 575
[40] Müller K-H 1997 *Physica C* **289** 123
[41] Müller K-H 1999 *Physica C* **312** 149 This paper also corrects typographical errors in expressions for the ac losses given in [40].
[42] Pearl J 1964 *Appl. Phys. Lett.* **5** 65
[43] Zeldov E, Clem J R, McElfresh M and Darwin M 1994 *Phys. Rev. B* **49** 9802
[44] Aslamazov L G and Lempicki S V 1983 *Zh. Eksp. Teor. Phys.* **84** 2216
[45] Vodolazov D Yu, Maksimov I L and Brandt E H 1999 *Europhys. Lett.* **48** 313
[46] Gradshteyn I S and Ryzhik I M 2000 *Table of Integrals, Series, and Products, 6th Ed*, ed A Jeffrey and D Zwillinger (Academic Press, San Diego)
[47] 1967 *Handbook of Mathematical Functions*, ed M Abramowitz and I A Stegun (National Bureau of Standards, Washington)
[48] 2005 *Mathematica, Version 5.2*, Wolfram Research, Inc., Champaign, IL
[49] Selfridge R B and Maxfield J E 1958 *A Table of the Incomplete Elliptic Integrals of the Third Kind* (Dover, New York)

[50] Byrd P F and Friedman M D 1954 *Handbook of Elliptic Integrals for Engineers and Physicists* (Springer, Berlin)
[51] Castro H, Dutoit B, Jacquier A, Baharami M and Rinderer L 1999 *Phys. Rev. B* **59** 596
[52] Hao Z, Clem J R, McElfresh M W, Civale L, Malozemoff A P and Holtzberg F 1991 *Phys. Rev. B* **43** 2844
[53] Babaei Brojeny A A and Clem J R 2005 *Supercond. Sci. Technol.* **18** 888
[54] Dam B, Huijbregtse J M, Klaassen F C, van der Geest R C F, Doornbos G, Rector J H, Testa A M, Freisem S, Martinez J C, Stäuble-Pümpin B and Griessen R 1999 *Nature* **399** 439
[55] Gutiérrez J, Llordés A, Gázquez J, Gibert M, Romà N, Ricart S, Pomar A, Sandiumenge F, Mestres N, Puig T and Obradors X 2007 *Nature Materials* doi:10.1038/nmat1893